RESEARCH ARTICLE

Lung cancer cells induce senescence and apoptosis of pleural mesothelial cells via transforming growth factor-beta1

**Zhi-Feng Miao · Wen-Ya Li · Zhen-Ning Wang ·
Ting-Ting Zhao · Ying-Ying Xu · Yong-Xi Song ·
Jin-Yu Huang · Hui-Mian Xu**

Abstract Pleural dissemination is commonly associated with metastatic advanced lung cancer. The injury of pleural mesothelial cells (PMCs) by soluble factors, such as transforming growth factor-beta1 (TGF-β1), is a major driver of lung cancer pleural dissemination (LCPD). In this study, we examine the effects of TGF-β1 on PMC injury and the ability of TGF-β1 inhibition to alleviate this effect both in vitro and in vivo. PMCs were co-cultured with the high TGF-β1-expressing lung cancer cell line A549 and with various TGF-β1 signaling inhibitors. Expression of cleaved-caspase 3, cleaved-caspase 9, p21, and p16 were evaluated by Western blot and immunofluorescent confocal imaging. Apoptosis was measured by 3-(4, 5-dimethylthiazol-2-yl)-2, 5-diphenyltrazoliumbromide assay and AnnexinV-propidium iodide (PI) staining. PMC senescence was assessed by staining for senescence-associated β-galactosidase (SA-β-Gal). The ability of lung cancer cells (LCCs) to adhere to injured PMCs was investigated using an LCC-PMC adhesion assay. In our mouse model, PMC injury status was monitored by hematoxylin–eosin (H&E) and Masson's trichrome staining. LCCs expressing high levels of TGF-β1 induce apoptosis and senescence of PMCs in a co-culture system. Injured PMCs adhere to LCCs, which may further promote LCPD.

Z.-F. Miao and W.-Y. Li contributed equally to this article.

Z.-F. Miao · Z.-N. Wang · Y.-X. Song · J.-Y. Huang · H.-M. Xu (✉)
Department of Surgical Oncology, The First Affiliated Hospital of
China Medical University, No. 155 North Nanjing Street, Heping
District, Shenyang, Liaoning 110001, China
e-mail: fengfeng19998@hotmail.com

W.-Y. Li
Department of Thoracic Surgery, The First Affiliated Hospital of
China Medical University, Shenyang, Liaoning, China

T.-T. Zhao · Y.-Y. Xu
Department of Breast Surgery, The First Affiliated Hospital of China
Medical University, Shenyang, Liaoning, China

Importantly, PMC monolayer injury could be reversed with TGF-β1 inhibitors. This was consistent with our in vivo data showing that the TGF-β1 inhibitor SB-431542 attenuated PMC barrier injury induced by A549 culture medium in our mouse model. Our study highlights the importance of TGF-β1 signaling in LCPD and establishes this signaling pathway as a potential therapeutic target in the disease.

Keywords Lung cancer · Pleural metastasis · TGF-β1 · Mesothelial cells · Senescence · Apoptosis

Introduction

Lung cancer is the most commonly diagnosed cancer and leading cause of cancer-related death worldwide [1, 2]. Pleural dissemination and metastasis of primary lung cancers are associated with advanced disease and is classified as stage IV according to the tumor–node–metastasis (TNM) staging system (7th edition) [3, 4]. In patients with non-small cell lung cancer (NSCLC) associated with pleural dissemination, the 5-year survival rate is 2 %, and the median survival time is 8 months [5]. Independent of the intial etiology, patients with malignant pleural effusion (MPE) have a median survival time of only 4 months [6]. To improve survival, a better understanding of the mechanisms governing lung cancer pleural dissemination (LCPD) is urgently needed.

According to Paget's "seed and soil" theory [7], metastasis occurs when tumor cells (seeds) encounter favorable local microenvironments (soil) where they can survive and rapidly proliferate. The specific site of cancer cell metastasis is not simply due to the anatomic location of the primary tumor or proximity to the secondary sites; instead, it involves interactions between tumor cells and the local microenvironment at the secondary site [8, 9]. Pleural mesothelial cells (PMC) form a monolayer covering the pleural cavity. This intact PMC

layer acts as a barrier and prevents lung cancer cells (LCCs) from infiltrating the sub-mesothelial connective tissue [10]. During metastasis, PMCs are exposed to high levels of soluble factors, including growth factors, cytokines, and chemokines, which are secreted by free LCCs within the MPE [11, 12]. Increased levels TGF-β1, interleukin (IL)-6, IL-8, and vascular endothelial growth factor in cases of MPE are correlated with higher TNM staging, increased occurrence of LCPD, and a worse prognosis [13–15]. However, whether the increase in LCPD is actually caused by soluble-factor-induced PMC injury, and which soluble factors result in the most damage, is currently unknown.

TGF-β1 is a 25-kDa homodimeric polypeptide implicated in a broad array of biological and pathological activities, including wound healing and fibrotic disease [16–18]. Additionally, its levels are strongly and rapidly up-regulated following multiple types of injury [19–21]. There are three mammalian TGF-β isoforms, TGF-β1, TGF-β2, and TGF-β3, that exert their functions via a cell surface receptor complex composed of type I (TGFBR1) and type II (TGFBR2) serine/threonine kinase receptors. Upon ligand binding, TGFBR2 recruits and phosphorylates TGFBR1, which in turn phosphorylates Smad2 or Smad3. Phosphorylated Smad2 or Smad3 binds to Smad4; these protein complexes then translocate from the cytoplasm to the nucleus where they can influence target gene expression [22].

In the present study, we demonstrate that TGF-β1, secreted by LCCs, induces apoptosis and senescence of PMCs. Furthermore, inhibition of TGF-β1 signaling attenuates TGF-β1-induced PMC injury in a co-culture system. This is consistent with our findings in animal models showing that inhibition of TGF-β1 signaling attenuates LCC-induced PMC monolayer damage in vivo. Our study highlights the importance of TGF-β1 signaling in LCPD and establishes this signaling pathway as a potential therapeutic target in the disease.

Materials and methods

Cell lines

The human mesothelial cell line HMR-SV5, human normal lung epithelial cell line GNHu27, and the LCC lines HUL42, A-549, GLC82, H441, PG49, and H1299 were all purchased from the cell bank of the Chinese Academy of Sciences (Shanghai, China). HUL42 and A-549 cells were cultured in Dulbecco's modified Eagle's medium (DMEM) medium containing 10 % fetal bovine serum (FBS). HMR-SV5, GLC82, H441, PG49, and H1299 were all cultured in RPMI-1640 medium containing 10 % FBS. All cells were incubated in a 5 % CO_2 atmosphere at 37 °C.

Animals

Male BALB/c nude mice (aged 8–10 weeks; weighing 20–22 g) were purchased from Vital River (Beijing, China). Mice were housed under sterile conditions and provided sterilized food and water. All animal protocols received prior approval from the China Medical University Animal Ethics Committee, and all experiments were performed in accordance with the appropriate guidelines.

Establishment of the PMC injury model

HMR-SV5 cells (5×10^5 cells/well) were seeded in a six-well plate. Once cells reached 80 % confluence, a co-culture insert was added (0.4 μm pore, Corning, USA), and 2×10^5 A549 cells were seeded into the upper chamber. The co-culture system was maintained in RPMI-1640 medium supplemented with 10 % FBS for the indicated times. For inhibition of the TGF-β1 signaling pathway, either TGF-β1 receptor inhibitor SB-431542 or TGF-β1 neutralizing antibody (neu-TGF) was added to the culture; cell culture medium was changed every other day. HMR-SV5 cells in the lower chamber were collected for further studies.

ELISA assay

Cytokine production was determined using a Quantikine human TGF-β1 enzyme-linked immunosorbent assay (ELISA) kit (R&D Systems) according to the manufacturer's instructions.

Western blot

Cells were incubated for 20 min on ice in 50 μL radioimmunoprecipitation assay buffer supplemented with 1 mM phenylmethylsulfonyl fluoride, 1 μg/mL leupeptin, 1 mM β-glycerophosphate, 2.5 mM sodium pyrophosphate, and 1 mM Na_3VO_4. Cells were then centrifuged for 20 min at $12,000 \times g$ at 4 °C. Next, 50 μg protein from each sample was resolved on 10 % sodium dodecyl sulfate (SDS) polyacrylamide gels and transferred to polyvinylidene fluoride (PVDF) membranes. Membranes were then blocked in Tris-buffered saline and Tween 20 (TBST) solution containing 4 % skim milk for 2 h at room temperature. Membranes were incubated with mouse monoclonal anti-cleaved caspase 3 (1:1000; CST, USA), mouse monoclonal anti-cleaved caspase 9 (1:1000; CST, USA), rabbit monoclonal anti-p21 (1:1000; CST, USA), or rabbit monoclonal anti-p16 (1:10000; Abcam, USA) primary antibodies in TBST solution overnight at 4 °C. Following overnight incubation, membranes were washed three times in TBST and then incubated with horseradish peroxidase-conjugated secondary antibodies (1:5000; Santa Cruz, USA) in TBST for 2 h at room temperature.

Membranes were incubated with ECL solution (Pierce, USA) for 1 min, and protein bands were visualized using the ECL chemiluminescence method.

Real-time PCR

Total RNA was extracted from cultured cells using Trizol reagent (Invitrogen, USA) and reverse-transcribed using the Transcriptor First Strand cDNA synthesis kit (Invitrogen, USA) according to the manufacturer's instructions. Quantitative real-time PCR reactions were performed using an iCycler iQ Real-Time PCR Detection System (Bio-Rad, USA) using the iQ SYBR Green Supermix (Bio-Rad). Real-time PCR data are expressed as relative messenger RNA (mRNA) expression quantified with Bio-Rad iCycler system software and normalized to β-actin levels.

Senescence-associated β-galactosidase staining

Senescence-associated β-galactosidase (SA-β-Gal) staining was performed using an SA-β-Gal Staining Kit (Genmed Scientifics Inc, USA) according to the manufacturer's protocol. Briefly, after co-culture treatment, HMR-SV5 cells were fixed in 4 % formaldehyde for 5 min and stained with SA-β-Gal staining solution at pH 6.0 for 16 h. Cells staining bright blue in color were considered positive. The experiment was repeated three times for each group.

MTT assay

PMC viability was assessed using an 3-(4, 5-dimethylthiazol-2-yl)-2, 5-diphenyltrazoliumbromide (MTT) assay. PMCs (approximately 1×10^4 cells/well) were seeded into 96-well culture plates and cultured in DMEM with 10 % FBS for 12–72 h. Cells were then incubated with 20 μL MTT (10 mg/mL) for 4 h at 37 °C, and 200 μL dimethyl sulfoxide was added for 20 min at room temperature to solubilize the formazan product. The optical density (OD) was determined using a spectrophotometer (Bio-800, Bio-Rad, USA) at a wavelength of 570 nm. Approximately 1×10^4 cells/well of untreated PMCs were cultured with serum-free DMEM medium as a control. Cell proliferation was calculated using the following equation:

$$\text{Cell proliferation rate } (\%) = \text{OD (Experimental group – Control group)} \Big/ \text{OD control group} \times 100\%$$

AnnexinV-propidium iodide staining

Apoptosis of HMR-SV5 cells was measured using an AnnexinV-propidium iodide (PI) apoptosis detection kit (Becton Dickinson, USA) according to the manufacturer's instructions. Briefly, cells were resuspended in 1× binding buffer at a concentration of 1×10^6/mL. Next, 5 μL Annexin V-fluorescein isothiocynate antibody and 5 μL PI were added; samples were incubated in the dark at room temperature for 15 min. After washing twice with 1× binding buffer, cell-surface staining was analyzed by flow cytometry (FACS Caliber, Becton Dickinson, USA). PMCs in the upper-right and the lower-right quadrants showed late- and early-stage apoptosis, respectively. For AnnexinV-PI confocal imaging, PMCs were cultured on a slide and subject to the same staining procedure. Images were obtained with an immunofluorescent microscope (FV1000, Olympus, Japan).

Immunofluorescent staining

Cells were fixed in 4 % paraformaldehyde in 20 mM HEPES (pH 7.4) for 20 min, rinsed three times, and incubated with a rabbit monoclonal anti-p16 antibody (1:500; Abcam, USA) for 1 h at room temperature. The membrane was then rinsed three times and incubated with a donkey anti-rabbit Alexa Fluor 594-conjugated secondary antibody for 30 min at room temperature in the dark. 4′,6-Diamidino-2-phenylindole was used for nuclear counterstaining. The stained cells were mounted and viewed under an immunofluorescent microscope (FV1000, Olympus, Japan).

Cell cycle analysis

The cell cycle was examined by a modified flow cytometric method. In brief, PMC cells were harvested at 24 and 48 h. Harvested cells were washed twice with phosphate-buffered saline (PBS) and fixed in ice-cold 70 % ethanol at 4 °C overnight. Ethanol-fixed cells were then stored at 4 °C for up to 1 month. Ethanol-fixed cells were centrifuged and washed once with PBS. The cell pellet was then suspended in 0.2 mL DNA extraction buffer (192 mL 0.2 M Na2HPO4 and 8 mL 0.1 M citric acid, pH 7.8) and incubated in a 37 °C shaker for 30 min. After incubation, cells were centrifuged at 1500 rpm for 10 min. The supernatant was carefully discarded. Then, the pellet was stained with a propidium iodide (PI) solution (0.08 mg PI, 0.1 % Triton X-100 and 0.1 mg/mL RNaseA in PBS) and incubated in the dark for 30 min at 37 °C. In total, 10,000 cells (adherent and non-adherent) were harvested. Cellular DNA contents were measured by exciting PI at 488 nm and measuring the emission at 580 nm using a BD canto II flow cytometer (BD Biosciences, San Jose, CA, USA).

3D artificial pleura model

PMCs were grown in 96-well plates pre-coated with 200 µL matrigel. Once PMCs reached 80 % confluence, co-culture inserts (0.4 µm pore, Corning, USA) were added. Approximately 2×10^4 A549 cells were seeded into the upper chamber. PMCs were co-cultured with A549 cells for the indicated length of time. Fresh culture medium was then added, and the LCC-PMC adhesion assay was performed.

LCC-PMC adhesion assay

The adhesion of tumor cells to PMCs was determined as previously described [15]. A549 cells were pretreated with or without 50 µg/mL RGD and stained with 15 µM calcein AM for 30 min at 37 °C. Subsequently, A549 cells (1×10^4/well) were added to the 24-well plates containing PMCs and incubated for 3 h at 37 °C. To remove non-adherent LCCs, the plates were then washed three times with 200 µL PBS. The fluorescent intensity in each well was recorded by spectrofluorometry using wavelengths of 485 and 535 nm for excitation and emission, respectively. As a positive control, PMC monolayers were seeded with labeled A549 cells and maintained for 30 min without any PBS wash steps. Untreated PMC monolayers were used as a negative control. Adhesion capability was calculated as follows:

$$\text{Adhesion capability} = \left(\text{fluorescence intensity of experimental group} - \text{negative control} \Big/ \text{fluorescence intensity of positive control} - \text{negative control} \right) \times 100\%$$

In vivo mesothelial cell injury models

Male BALB/c nude mice were divided into control and treatment groups ($n = 10$ per group). Mice in both groups received 1 mL A549 cell-conditioned medium (CM) by intrapleural injection (i.p.) at a left costophrenic angle prior to being anesthetized via inhalation of isoflurane. Mice in the treatment group were also injected with 0.5 mL 1 µM SB-431542 on days 1 and 3 after CM inoculation; as a comparison, mice in the control group received two i.p. injections of 0.5 mL PBS. Two weeks post-inoculation, mice in each group were killed by cervical dislocation. The pleural wall, pleura, and diaphragm were excised, fixed, and embedded for H&E and Masson's trichrome stain.

Masson's trichrome staining

Masson's trichrome staining was performed as previously described [14]. Briefly, 4-µm sections were deparaffinized and hydrated by sequential incubations in xylene and ethanol. After washing, sections were placed in Bouin's fixative for 1 h at room temperature, transferred to 4 % ferric ammonium sulfate for 5 min at 50 °C, and rapidly rinsed with distilled water at 50 °C. Slides were then immersed in 0.1 % acid fuchsin for 1 min, gently rinsed five times by repeated immersion in water, placed in 1 % phosphomolybdic acid for 10 min, and stained for 90 s in 0.25 % light green/0.5 % phosphomolybdic acid. The slides were then washed in water until the rinses became clear, dehydrated in graded ethanol, cleared with xylene, and covered with coverslips using neutral resin.

Statistical analysis

All statistical analyses were performed using SPSS version 16.0 software (SPSS Inc., USA). Continuous variable data obtained from two separate experiments were examined by t test. Continuous variable data obtained from three or more separate experiments were examined by ANOVA test. Data are expressed as mean±SD. Statistical significance was set at $p < 0.05$.

Results

High expression of TGF-β1 in human LCC lines

We measured cytoplasmic expression of TGF-β1 in six LCC lines (HUL42, A549, GLC82, H441, H1299, and PG49) by Western blot analysis. TGF-β1 was detected in four of the six cell lines, with the highest expression detected in A549 cells (Fig. 1a). We also performed real-time PCR to assess TGF-β1 mRNA levels in each of the cell lines; quantitative PCR data were consistent with our Western blot analysis. A549 cells showed 3.6±0.25-fold higher expression of TGF-β1 mRNA compared to HUL42 cells (Fig. 1b, $P < 0.05$). Based on these results, we chose A549 cells for subsequent functional studies. TGF-β1 level was compared among lung cancer cells (A549), normal lung epithelial cells (GNHu27) as well as PMCs at protein levels (Fig. 1c). PMCs exhibited higher TGF-β1 expression compared with GNHu27 cells (3.52±0.25-fold, $P < 0.05$). TGF-β1 expression was also compared among untreated PMCs, PMCs co-cultured with A549 cells, and PMCs co-cultured with GNHu27. No significant difference in
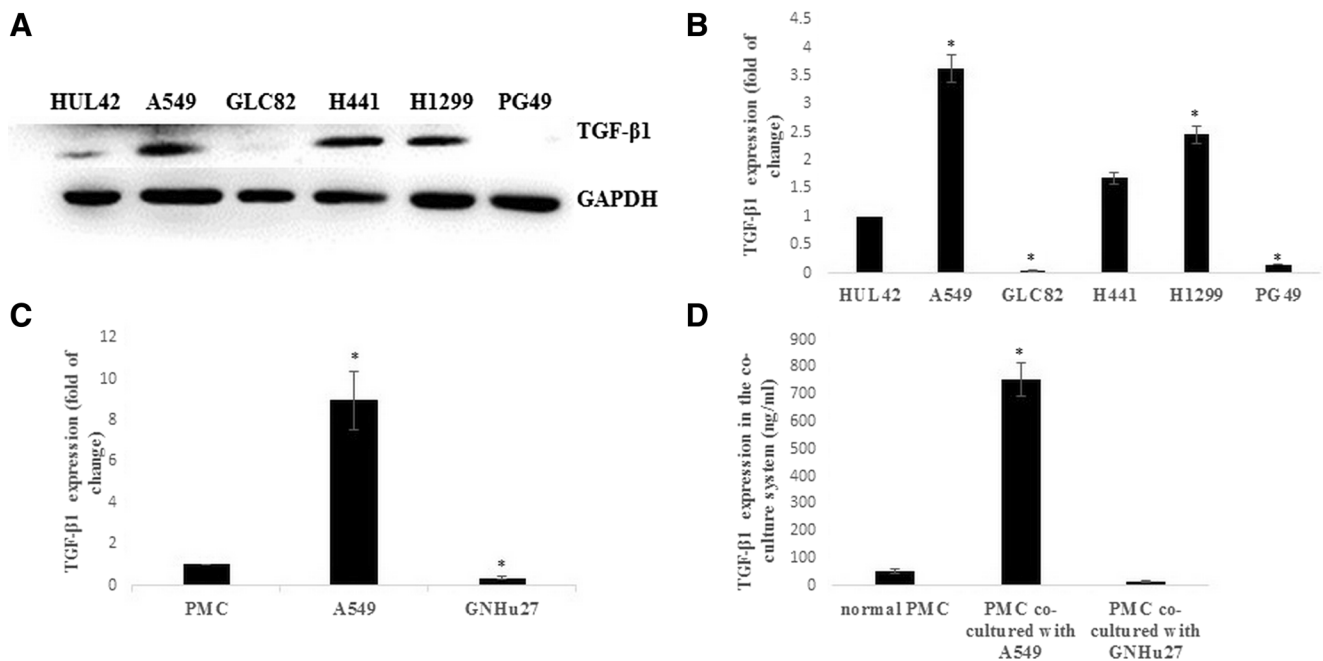
Fig. 1 High expression of TGF-β1 in human LCC lines. **a** Western blot showing the expression of TGF-β1 in six LCC lines. GAPDH served as a protein loading control. **b** Expression of TGF-β1 in six LCC lines was analyzed by real-time PCR. Results are expressed as fold of change (mean±SD, *P<0.05 compared with HUL-42). **c** Expression of TGF-β1 were compared among A549, GNHu27 as well as PMCs by ELISA assay. Results are expressed as fold of change (mean±SD, *P<0.05 compared with PMCs). **d** Expression of TGF-β1 were evaluated in normal PMCs, PMCs co-cultured with A549 cells and PMCs co-cultured with GNHu27 cells by ELISA assay. (Results are expressed as mean±SD, *P<0.05 compared with untreated PMCs)

TGF-β1 level was detected between untreated PMCs and PMCs co-cultured with GNHu27 (Fig. 1d, P>0.05).

LCC lines induce PMC injury and promote tumor cell adhesion

The expression of proteins related to senescence and apoptosis were analyzed by Western blot (Fig. 2a). We examined expression of senescence-related proteins p16 and p21 and apoptosis-related proteins cleaved-caspase-3 and cleaved-caspase-9 in PMCs co-cultured with A549 cells; comparisons were made against PMCs not cultured in the presence of A549 cells. Expression of p16 and p21 did not show a significant increase from 12 to 48 h. In contrast, expression of apoptosis-related proteins was elevated and reached a maximum by 48 h. MTT assay indicated that proliferation of PMCs was reduced following 12 h co-culture with A549 cells; by 48 h, proliferation was completely inhibited. Untreated, control PMCs displayed normal levels of cell proliferation. Proliferation rates of co-cultured PMCs were as follows: 12 h, 20.8± 4.2 %; 24 h, 21.1±5.1 %; and 48 h, 8.4±1.4 % (all P<0.05 compared to normal PMCs at each time point, Fig. 2b). Apoptotic became more apparent after longer periods of co-culture incubation. The expression of senescence-related proteins peaked by 12 h. We expanded on this observation by performing SA-β-Gal staining. As shown in Fig. 2c, co-cultured PMCs showed distinctive senescent morphology

and bright blue staining, indicative of positive β-Gal expression (red arrow). The expression of p16 protein was also investigated by immunofluorescent staining (Fig. 2d). After 12 h of co-culture, PMCs exhibited significantly increased p16 expression, which was found located both in the center and at the periphery of the nucleus. Apoptosis was examined by Annexin V-PI double staining (Fig. 2e). PMC apoptosis was more apparent after 24 h of co-culture. The apoptosis rates of normal and co-cultured PMCs were as follows: normal PMCs, 0.52±0.01 % (early stage) and 2.19±0.03 % (late stage); co-cultured PMCs, 4.78±0.16 % (early stage) and 10.97±0.74 % (late stage) (both P<0.05). Cell cycle was also assayed by FACS, co-cultured PMC exhibited more apparent G1/S and G2/M arrest (Fig. 2f).

In LCC-PMC adhesion assays, the attachment of co-cultured PMCs to the 3D artificial pleura model was significantly greater than that of untreated PMCs at multiple time points (22.6±1.47 % for 12 h; 54.8±3.5 % for 24 h; 56.7± 4.44 % for 48 h; all P<0.05 compared to normal PMCs, Fig. 2g).

Inhibition of TGF-β1 signaling reduces LCC-induced PMC injury and inhibits tumor cell adhesion

Multiple TGF-β1 inhibitors were tested in our co-culture system. Following 48 h of treatment, both SB-431542 and neu-TGF-β1 abrogated A549-induced PMC senescence and
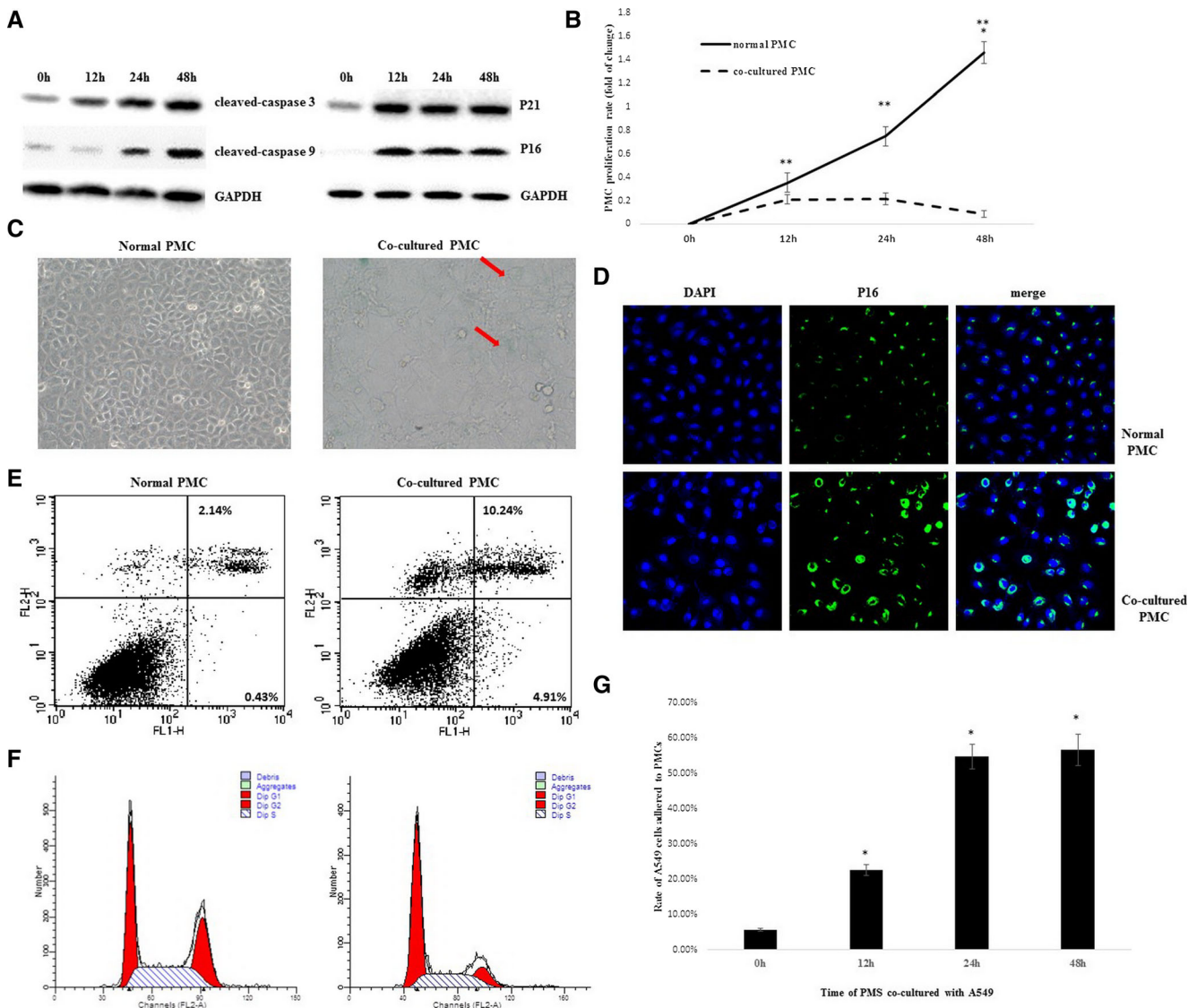
Fig. 2 LCC lines induce PMC injury and promote tumor cell adhesion. **a** Western blot showing the expression of senescence- and apoptosis-related proteins in PMCs co-cultured with A549 cells. GAPDH served as a protein loading control. **b** PMC proliferation was analyzed by MTT assay. Results are expressed as fold of change (mean±SD, *P<0.05 compared with normal PMC; **P<0.05 compared with co-cultured PMC at indicated time interval). **c** SA-β-Gal staining of PMCs co-cultured with A549 cells (red arrow indicates senescent PMCs). **d** Immunofluorescence analysis of p16 expression in PMCs co-cultured with A549 cells (p16,

green staining; 4′,6-diamidino-2-phenylindole, blue staining; magnification, ×600). **e** Annexin V-PI double staining shows early- and late-stage apoptosis of PMCs in the co-culture system (dots in right-lower quadrant indicate early stage apoptosis of PMCs; dots in right-upper quadrant indicate late stage apoptosis). **f** Cell cycle assayed shows G1/S and G2/M arrest of PMCs in the co-culture system. **g** Rate of A549 cells adhered to confluent PMCs. (Data are expressed as mean±SD, *P<0.05 compared with co-cultured PMCs at 0 h

apoptosis (Fig. 3a). To further investigate the impact of TGF-β1 inhibition on LCC adhesion, we established a 3D artificial pleura model. As shown in Fig. 3b, both SB-431542 and neu-TGF-β1 significantly reduced (66.4 and 54.6 %, respectively; P<0.05) the attachment of A549 cells in the 3D artificial pleura model. To investigate if TGF-β1 inhibitors exert a direct effect on PMCs, their proliferative capacity in the presence of SB-431542 or neu-TGF-β1was assessed. MTT assays showed reduced proliferation in A549 cells treated with neu-TGF-β1 (0.75±0.03-fold compared to untreated

A549; P<0.05; Fig. 3c). In contrast, low-dose SB-431542 did not directly affect proliferation of A549 cells (0.93±0.05-fold compared to untreated A549; P>0.05; Fig. 3c).

Inhibition of TGF-β1 signaling attenuates PMC-mediated injury in vivo

To investigate the effects of TGF-β1 inhibition on PMC-mediated injury in vivo, nude mice were inoculated (i.p.) with conditioned medium (CM) from A549 cells and then injected

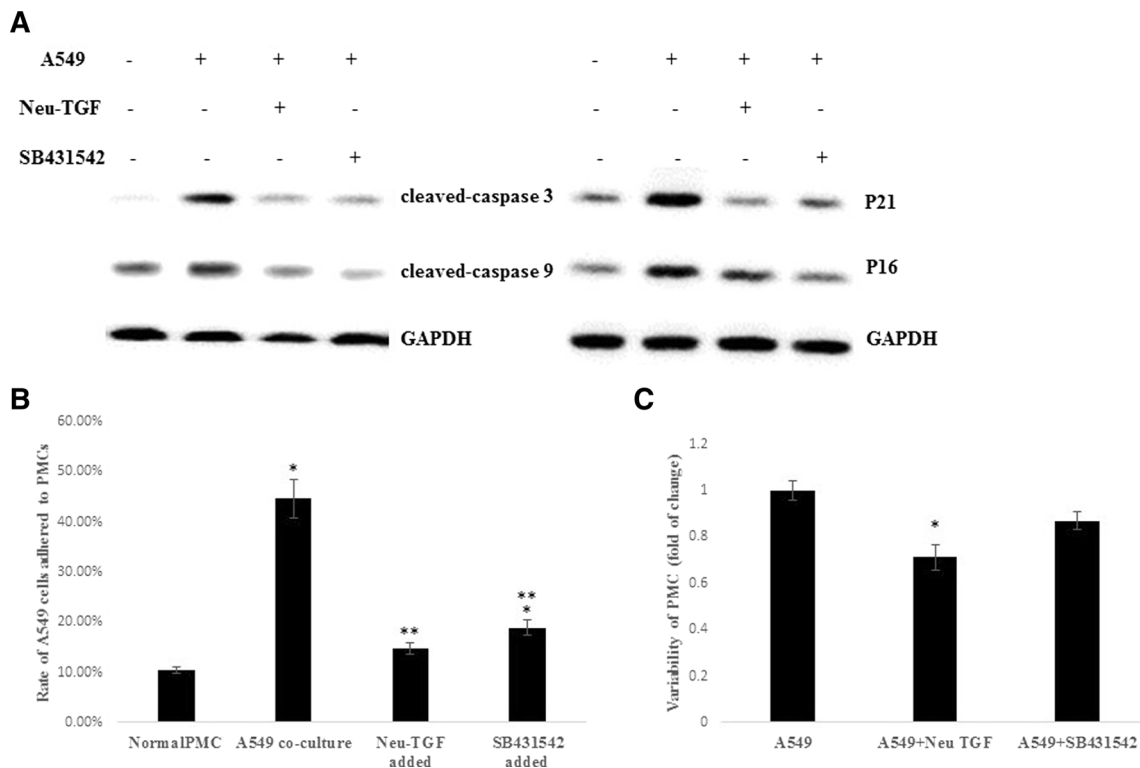Fig. 3 Inhibition of TGF-β1 signaling reduces LCC-induced PMC injury and inhibits tumor cell adhesion. **a** Western blot showing expression of senescence- and apoptosis-related proteins in PMCs co-cultured with A549 cells. GAPDH served as a protein loading control. TGF-β1 signaling inhibitors were added to the co-culture system where indicated. **b** Numbers of A549 cells attached to confluent PMCs. (Data are expressed as mean±SD, *$P<0.05$ compared with normal PMC; **$P<0.05$ compared with PMCs co-cultured with A549 cells). **c** MTT assay of A549 cells treated with different reagents. (Data are expressed as fold change relative to untreated A549 cells, *$P<0.05$ compared with untreated A549 cells)
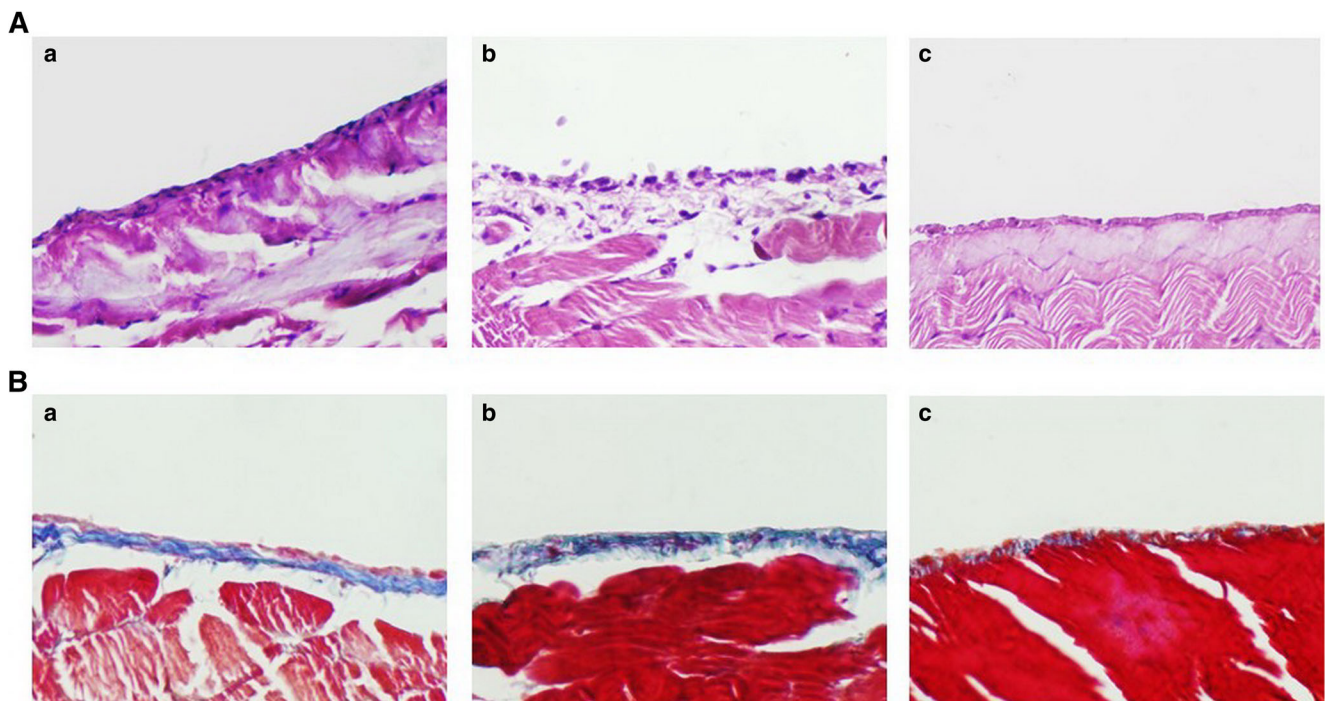

Fig. 4 Blockade TGF-β1 signaling inhibits PMC injury in vivo. **a** H&E staining of the pleura of mice in the control group (*right*, **c**), untreated mice (*middle*, **b**), and in the SB431542-treated group (*left*, **a**) (magnification, ×400). **b** Masson's trichrome staining showing the integrity of the PMC monolayer and pleural collagen fiber exposure in mice in the control group (*right*, **b**) and in the SB431542-treated group (*left*, **a**) (magnification, ×400)

with either 1 mL 1 μM SB-431542 or PBS. This was followed by HE and Masson's trichrome staining (Fig. 4). In the control group (A549 cell CM with PBS), the PMC monolayer became discontinued, and the submesothelial collagenous zone became exposed to the chest cavity—typical pathological changes associated with pleura injury (Fig. 4a); additionally, Masson's trichrome staining showed evidence of senescence and apoptosis. In contrast, treatment with SB431542 protected the PMC monolayer from injury (Fig. 4b).

Discussion

Although mesothelial cells can prevent against tumor invasion, they may become damaged in response to soluble factors released by tumor cells during metastasis [23, 24]. Damaged PMCs become hemispherical in shape and undergo exfoliation, which results in exposure of sub-mesothelial connective tissue and collagen fiber [25, 26]. Thus, naked areas of submesothelial connective tissue become directly exposed to tumor cells and may serve as a favorable "soil" to promote tumor dissemination. MPE is a common occurrence in lung cancer patients with advanced TNM staging, and it is correlated with lung cancer metastasis and poor prognosis [11, 27]. While several soluble factors may induce PMC injury, in this study, we specifically focus on TGF-β1.

TGF-β1 plays a role in a number of normal and pathological processes, including fibrotic disease, wound healing, stroma reconstruction, tumorigenesis, and metastasis [19, 20]. TGF-β1 regulates cellular senescence, apoptosis, and differentiation via the TGF-β/Smad pathway [28, 29]. However, a role for TGF-β1 in LCPD is currently unknown. To address this question, we co-cultured PMCs with the high TGF-β1-expressing A549 LCC line. We also evaluated whether TGF-β1 signaling blockade inhibited LCPD both in vitro and in vivo.

We examined TGF-β1 expression in six human LCC lines and found the highest expression level in A549 cells. PMC proliferation was inhibited by co-culture with A549 cells in a time-dependent manner. Co-culture also increased senescence, apoptosis, and attachment of PMCs. Importantly, these effects were attenuated in the presence of a TGF-β inhibitor, establishing TGF-β1 signaling as a potential therapeutic target in the disease.

Inhibition of TGF-β1 signaling to block cancer metastasis has been the focus of several studies in recent years [30, 31]. Treatment of TGFβR-expressing cells with SB-431542 (3–10 μM) reduces both proliferation and migration/invasion ability [32, 33]. In our study, low-dose (1 μM) SB-431542 had no direct effect on PMC proliferation but markedly attenuated LCC-induced PMC injury in a co-culture system (Fig. 3). Another inhibitor, neu-TGF-β1, was capable of

exerting a direct cytotoxic effect on PMCs. Our in vitro findings were supported by our in vivo experiments as well. It should be noted that inhibition of TGF-β1 only partially attenuated LCC-induced PMC injury. This suggests that additional LCC-secreted soluble factors may also contribute to this process. Thus, additional research to identify such factors should be the focus of future research.

In conclusion, our results demonstrate that LCCs invading the pleural cavity can secrete soluble factors, such as TGF-β1, that induce senescence and apoptosis of PMCs and promote LCPD. Our study highlights the importance of TGF-β1 signaling in LCPD and establishes this signaling pathway as a potential therapeutic target in the disease.

References

1. Siegel R, Ma J, Zou Z, Jemal A. Cancer statistics, 2014. CA Cancer J Clin. 2014;64:9–29.
2. Ferlay J, Soerjomataram I, Ervik M, Dikshit R, Eser S, Mathers C, et al. GLOBOCAN 2012 v1.0, Cancer incidence and mortality worldwide: IARC CancerBase No. 11. Lyon, France: International Agency for Research on Cancer 2013. http://globocan.iarc.fr.
3. Goldstraw P, Crowley J, Chansky K, Giroux DJ, Groome PA, Rami-Porta R, et al. International Association for the Study of Lung Cancer International Staging Committee; participating institutions. The IASLC lung cancer staging project: proposals for the revision of the TNM stage groupings in the forthcoming (seventh) edition of the TNM Classification of malignant tumours. J Thorac Oncol. 2007;2:706–14.
4. Postmus PE, Brambilla E, Chansky K, Crowley J, Goldstraw P, Patz Jr EF, et al. International Association for the Study of Lung Cancer International Staging Committee; cancer research and biostatistics; observers to the committee; participating institutions. The IASLC lung cancer staging project: proposals for revision of the M descriptors in the forthcoming (seventh) edition of the TNM classification of lung cancer. J Thorac Oncol. 2007;2:686–93.
5. Detterbeck FC, Boffa DJ, Tanoue LT. The new lung cancer staging system. Chest. 2009;136:260–71.
6. Heffner JE, Klein JS. Recent advances in the diagnosis and management of malignant pleural effusions. Mayo Clin Proc. 2008;83:235–50.
7. Mathot L, Stenninger J. Behavior of seeds and soil in the mechanism of metastasis: a deeper understanding. Cancer Sci. 2012;103:626–31.
8. Morgan SC, Parker CC. Local treatment of metastatic cancer—killing the seed or disturbing the soil? Nat Rev Clin Oncol. 2011;8:504–6.
9. Langley RR, Fidler IJ. The seed and soil hypothesis revisited—the role of tumor-stroma interactions in metastasis to different organs. Int J Cancer. 2011;128:2527–35.
10. Nasreen N, Mohammed KA, Sanders K, Hardwick J, Van Horn RD, Sriram PS, et al. Pleural mesothelial cell (PMC) defense mechanisms against malignancy. Oncol Res. 2003;14:155–61.

11. Froudarakis ME. Pleural effusion in lung cancer: more questions than answers. Respiration. 2012;83:367–76.
12. Atanackovic D, Cao Y, Kim JW, Brandl S, Thom I, Faltz C, et al. The local cytokine and chemokine milieu within malignant effusions. Tumour Biol. 2008;29:93–104.
13. Duysinx BC, Corhay JL, Hubin L, Nguyen D, Henket M, Louis R. Diagnostic value of interleukine-6, transforming growth factor-beta 1 and vascular endothelial growth factor in malignant pleural effusions. Respir Med. 2008;102:1708–14.
14. Ishii H, Yazawa T, Sato H, Suzuki T, Ikeda M, Hayashi Y, et al. Enhancement of pleural dissemination and lymph node metastasis of intrathoracic lung cancer cells by vascular endothelial growth factors (VEGFs). Lung Cancer. 2004;45:325–37.
15. Cheng D, Kong H, Li Y. Prognostic values of VEGF and IL-8 in malignant pleural effusion in patients with lung cancer. Biomarkers. 2013;18:386–90.
16. Samarakoon R, Overstreet JM, Higgins PJ. TGF-β signaling in tissue fibrosis: redox controls, target genes and therapeutic opportunities. Cell Signal. 2013;25:264–8.
17. Cencetti F, Bernacchioni C, Tonelli F, Roberts E, Donati C, Bruni P. TGFβ1 evokes myoblast apoptotic response via a novel signaling pathway involving S1P4 transactivation upstream of Rho-kinase-2 activation. FASEB J. 2013;27:4532–46.
18. Pineda JR, Daynac M, Chicheportiche A, Cebrian-Silla A, Sii Felice K, Garcia-Verdugo JM, et al. Vascular-derived TGF-β increases in the stem cell niche and perturbs neurogenesis during aging and following irradiation in the adult mouse brain. EMBO Mol Med. 2013;5:548–62.
19. Senturk S, Mumcuoglu M, Gursoy-Yuzugullu O, Cingoz B, Akcali KC, Ozturk M. Transforming growth factor-beta induces senescence in hepatocellular carcinoma cells and inhibits tumor growth. Hepatology. 2010;52:966–74.
20. Bian Y, Hall B, Sun ZJ, Molinolo A, Chen W, Gutkind JS, et al. Loss of TGF-β signaling and PTEN promotes head and neck squamous cell carcinoma through cellular senescence evasion and cancer-related inflammation. Oncogene. 2012;31:3322–32.
21. Klein S, Klösel J, Schierwagen R, Körner C, Granzow M, Huss S, et al. Atorvastatin inhibits proliferation and apoptosis, but induces senescence in hepatic myofibroblasts and thereby attenuates hepatic fibrosis in rats. Lab Invest. 2012;92:1440–50.
22. Moustakas A, Heldin CH. The regulation of TGF-β signal transduction. Development. 2009;136:3699–714.
23. Sandoval P, Jiménez-Heffernan JA, Rynne-Vidal A, Pérez-Lozano ML, Gilsanz A, Ruiz-Carpio V, et al. Carcinoma-associated fibroblasts derive from mesothelial cells via mesothelial-to-mesenchymal transition in peritoneal metastasis. J Pathol. 2013;231:517–31.
24. Na D, Lv ZD, Liu FN, Xu Y, Jiang CG, Sun Z, et al. Gastric cancer cell supernatant causes apoptosis and fibrosis in the peritoneal tissues and results in an environment favorable to peritoneal metastases, in vitro and in vivo. BMC Gastroenterol. 2012;12:34.
25. Jiang CG, Lv L, Liu FR, Wang ZN, Liu FN, Li YS, et al. Downregulation of connective tissue growth factor inhibits the growth and invasion of gastric cancer cells and attenuates peritoneal dissemination. Mol Cancer. 2011;10:122.
26. Na D, Lv ZD, Liu FN, Xu Y, Jiang CG, Sun Z, et al. Transforming growth factor beta1 produced in autocrine/paracrine manner affects the morphology and function of mesothelial cells and promotes peritoneal carcinomatosis. Int J Mol Med. 2010;26:325–32.
27. Yeh HH, Chang WT, Lu KC, Lai WW, Liu HS, Su WC. Upregulation of tissue factor by activated Stat3 contributes to malignant pleural effusion generation via enhancing tumor metastasis and vascular permeability in lung adenocarcinoma. PLoS One. 2013;8:e75287.
28. Elliot SJ, Karl M, Berho M, Xia X, Pereria-Simon S, Espinosa-Heidmann D, et al. Smoking induces glomerulosclerosis in aging estrogen-deficient mice through cross-talk between TGF-beta1 and IGF-I signaling pathways. J Am Soc Nephrol. 2006;17:3315–24.
29. Kawakita T, Espana EM, Higa K, Kato N, Li W, Tseng SC. Activation of Smad-mediated TGF-β signaling triggers epithelial-mesenchymal transitions in murine cloned corneal progenitor cells. J Cell Physiol. 2013;228:225–34.
30. Dhasarathy A, Phadke D, Mav D, Shah RR, Wade PA. The transcription factors snail and slug activate the transforming growth factor-beta signaling pathway in breast cancer. PLoS One. 2011;6:e26514.
31. Liu IM, Schilling SH, Knouse KA, Choy L, Derynck R, Wang XF. TGFbeta-stimulated Smad1/5 phosphorylation requires the ALK5 L45 loop and mediates the pro-migratory TGFbeta switch. EMBO J. 2009;28:88–98.
32. Mandel K, Seidl D, Rades D, Lehnert H, Gieseler F, Hass R, et al. Characterization of spontaneous and TGF-β-induced cell motility of primary human normal and neoplastic mammary cells in vitro using novel real-time technology. PLoS One. 2013;8:e56591.
33. Ehata S, Hanyu A, Hayashi M, Aburatani H, Kato Y, Fujime M, et al. Transforming growth factor-beta promotes survival of mammary carcinoma cells through induction of antiapoptotic transcription factor DEC1. Cancer Res. 2007;67:9694–703.